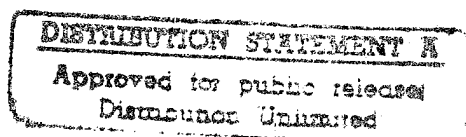# Comparison of Composite Rotor Blade Models: A Coupled-Beam Analysis and an MSC/NASTRAN Finite-Element Model

Robert V. Hodges, Mark W. Nixon,
and Lawrence W. Rehfield

MARCH 1987

19951102 013

NASA

Comparison of Composite Rotor Blade Models: A Coupled-Beam Analysis and an MSC/NASTRAN Finite-Element Model

Robert V. Hodges and Mark W. Nixon

Aerostructures Directorate
USAARTA-AVSCOM
Langley Research Center
Hampton, Virginia

Lawrence W. Rehfield

Georgia Institute of Technology
Atlanta, Georgia

Accesion For

NTIS CRA&I	☑	
DTIC TAB	☐	
Unannounced	☐	
Justification		

By DTIC-AI mumw
Distribution / 11-2-95

Availability Codes		
Dist	Avail and / or Special	
A-1		

Summary

A methodology was developed by Lawrence W. Rehfield for the structural analysis of composite rotor blades. This coupled-beam analysis is relatively simple to use compared with the alternative analysis techniques. The beam analysis was developed for thin-wall single-cell rotor structures and includes the effects of elastic coupling achieved through unbalanced ply orientation.

This paper demonstrates the effectiveness of the new composite-beam analysis method. This is accomplished through comparison of the results of the coupled-beam analysis with those of an established baseline analysis technique. The baseline analysis tool is an MSC/NASTRAN finite-element model built up from anisotropic shell elements. Deformations for three linear static load cases are compared. These loads are centrifugal force at design rotor speed, applied torque, and lift for an ideal rotor in hover. A D-spar designed to twist under axial loading is the subject of the analysis.

At design rotor speed the finite-element analysis and the coupled-beam analysis indicate, respectively, 14° and 15° of twist at the spar tip. The finite-element model indicates less twist due to rigid boundary conditions and wall thickness considerations. A similar trend is indicated by the applied-torque load case. In the applied-lift load case, vertical deflections and twist indicated by both analysis methods are essentially the same. Results indicate the coupled-beam analysis is well within engineering accuracy.

The results presented demonstrate that moderate variations in spar twist can be achieved by varying the rotor rotational speed. The analysis also provides a new and convenient approach for obtaining the extensional, torsional, and bending engineering stiffnesses.

Introduction

A methodology was developed by Rehfield for the structural analysis of composite rotor blades (ref. 1). The beam force-deformation relationship is controlled by cross-section properties that are easily defined line integrals around the rotor spar. This coupled-beam analysis is relatively simple to use compared with alternative analysis techniques. The beam analysis was developed for thin-wall single-cell rotor structures. It includes the effects of elastic coupling achieved through unbalanced ply orientation.

In light of its potential, applications of the coupled-beam analysis are needed. One application is to design a rotor blade that would change twist as a function of rotor speed. A scale model rotor blade described in this report was designed to demonstrate this coupling. The spar from that preliminary design effort was selected as the subject of the analytical study presented here.

The purpose of this paper is to demonstrate the effectiveness of the new composite-beam methodology. This is accomplished by analysis of the D-spar through comparison of results from use of the coupled-beam analysis and an established analysis technique.

Nomenclature

$B_{y,x}$	beam flapwise curvature, in^{-1}
$B_{z,x}$	beam chordwise curvature, in^{-1}
C_{ij}	coupled-beam stiffness terms (from ref. 1)
E_{11}	lamina longitudinal modulus, psi
E_{22}	lamina transverse modulus, psi
EA	beam uncoupled extensional stiffness, lb
EI_c	beam uncoupled chordwise bending stiffness, lb-in^2
EI_f	beam uncoupled flapwise bending stiffness, lb-in^2
G_{12}	lamina shear modulus, psi
GK	beam uncoupled torsional stiffness, lb-in^2
L	elastic beam length, in.
M_x	beam torsional moment, in-lb
M_y	beam flapwise bending moment, in-lb
M_z	beam chordwise bending moment, in-lb
N_x	beam axial force (centrifugal force), lb
Q_y	beam shear, chordwise, lb
Q_z	beam shear, flapwise, lb
S_{ij}	coupled-beam compliance terms (from ref. 1)
$U_{,x}$	beam extension strain
$V_{,x}$	beam chordwise shear strain
$W_{,x}$	beam flapwise shear strain
w	distributed beam load, lb/in.
z_{tip}	tip deflection due to beam load, in.

ν_{12} lamina primary Poisson ratio

$\phi_{,x}$ beam twist rate, deg/in.

Approach

The baseline analysis tool selected is MSC/NASTRAN (refs. 2 to 4). The NASTRAN finite-element model is built up from anisotropic shell elements. Deformations for three linear static load cases are compared. These loads are centrifugal force, ideal lift, and applied torque.

The model rotor blade is shown in figure 1. The spar from this design (fig. 2) is the subject of the analysis. The finite-element model and the beam-element model are developed from the same rotor geometry. The spar has a 35.23-in. radius. The analytical model is rigid to radial station 5.23 in. and has a constant cross section from station 5.23 in. to 35.23 in. The model is divided into 50 spanwise segments (0.60 in. each). The cross section is defined by 16 nodes.

For comparison purposes the spar is considered to be a cantilever and is analyzed as a linear static structure. It is essentially rigid from the center of rotation to the spar root. In the finite-element model a rigid element acts as an end rib connecting the outboard end of the beam element to quadrilateral elements at station 5.23 in.

The spar is a high strain graphite and toughened epoxy composite made of Hercules IM6 fiber with Ciba-Geigy R6376 resin. It has a 6-ply layup $[+20/-70/+20/-70_2/+20]$, with $0°$ oriented to the pitch axis. The cured ply thickness is 0.0055 in. The orthotropic material properties are shown in table I.

The beam force-deformation relationship according to reference 1 is

$$\begin{bmatrix} N_x \\ Q_y \\ Q_z \\ M_x \\ M_y \\ M_z \end{bmatrix} = [C_{ij}] \begin{bmatrix} U_{,x} \\ V_{,x} \\ W_{,x} \\ \phi_{,x} \\ B_{y,x} \\ B_{z,x} \end{bmatrix} \qquad (1)$$

where $[C_{ij}]$ is a 6 by 6 beam stiffness matrix. The terms in the stiffness matrix are evaluated for the D-spar (table II). The nonzero coupling terms (off-diagonal terms) are $C_{14}, C_{25},$ and C_{36}. Thus, coupling exists between extension and twist, between flapwise shear and chordwise bending, and between chordwise shear and flapwise bending. Equation (1) can then be written as

$$N_x = C_{11}U_{,x} + C_{14}\phi_{,x} \text{ lb} \qquad (2)$$

$$Q_y = C_{22}V_{,x} + C_{25}B_{y,x} \text{ lb} \qquad (3)$$

$$Q_z = C_{33}W_{,x} + C_{36}B_{z,x} \text{ lb} \qquad (4)$$

$$M_x = C_{14}U_{,x} + C_{44}\phi_{,x} \text{ in-lb} \qquad (5)$$

$$M_y = C_{25}V_{,x} + C_{55}B_{y,x} \text{ in-lb} \qquad (6)$$

$$M_z = C_{36}W_{,x} + C_{66}B_{z,x} \text{ in-lb} \qquad (7)$$

In order to apply forces and to calculate beam deformations, it is necessary to invert equation (1). This inversion yields the compliance relationship

$$\begin{bmatrix} U_{,x} \\ V_{,x} \\ W_{,x} \\ \phi_{,x} \\ B_{y,x} \\ B_{z,x} \end{bmatrix} = [S_{ij}] \begin{bmatrix} N_x \\ Q_y \\ Q_z \\ M_x \\ M_y \\ M_z \end{bmatrix} \qquad (8)$$

where $[S_{ij}] = [C_{ij}]^{-1}$. For this particular case, the inversion can be accomplished if equations (2) to (7) are broken into three pairs of equations with three unknowns each. The following expressions for the nonzero compliance terms result:

$$\left. \begin{aligned} S_{11} &= \left(C_{11} - \frac{C_{14}^2}{C_{44}} \right)^{-1} \\ S_{22} &= \left(C_{22} - \frac{C_{25}^2}{C_{55}} \right)^{-1} \\ S_{33} &= \left(C_{33} - \frac{C_{36}^2}{C_{66}} \right)^{-1} \\ S_{44} &= \left(C_{44} - \frac{C_{14}^2}{C_{11}} \right)^{-1} \\ S_{55} &= \left(C_{55} - \frac{C_{25}^2}{C_{22}} \right)^{-1} \\ S_{66} &= \left(C_{66} - \frac{C_{36}^2}{C_{33}} \right)^{-1} \\ S_{14} &= -\left(\frac{C_{14}}{C_{44}} \right) S_{11} \\ S_{25} &= -\left(\frac{C_{25}}{C_{55}} \right) S_{22} \\ S_{36} &= -\left(\frac{C_{36}}{C_{66}} \right) S_{33} \end{aligned} \right\} \qquad (9)$$

Substituting the table II values into equations (9) yields the beam compliance values given in table III. The beam cross-section force deformation can then be written in terms of beam strains and curvatures as a function of applied loads:

$$U_{,x} = S_{11}N_x + S_{14}M_x \tag{10}$$

$$V_{,x} = S_{22}Q_y + S_{25}M_y \tag{11}$$

$$W_{,x} = S_{33}Q_z + S_{36}M_z \tag{12}$$

$$\phi_{,x} = S_{14}N_x + S_{44}M_x \ \text{deg/in.} \tag{13}$$

$$B_{y,x} = S_{25}Q_y + S_{55}M_y \ \text{in}^{-1} \tag{14}$$

$$B_{z,x} = S_{36}Q_z + S_{66}M_z \ \text{in}^{-1} \tag{15}$$

Application of Analysis

Centrifugal Load Case

The model rotor (fig. 1) has a design rotor speed of 2077 rpm and weighs 0.0123 lb/in. of span. These values are used to calculate the centrifugal force N_x applied to the spar:

$$N_x = 934.4 - 0.75287x^2 \ \text{lb} \tag{16}$$

where x is measured from station 5.23 in.

The material density in the finite-element model is selected to produce the same weight per unit length as the model rotor (0.0123 lb/in.). This is verified by comparing the root centrifugal force calculated by the finite-element model with the root centrifugal force calculated by equation (16).

Lifting Load Case

The ideal rotor in hover has a triangular lift distribution from radial station 5.23 in. to 35.23 in. The total magnitude of the lift load is selected to be 10 lb. The shears and moments produced by the triangular lift and the blade weight are calculated by linear statics. The load w due to lift and blade weight can be written in terms of x as

$$w = 0.02222x - 0.0123 \ \text{lb/in.} \tag{17}$$

Integrating once gives the shear

$$Q_z = 0.01111x^2 - 0.0123x - 9.631 \ \text{lb} \tag{18}$$

Integrating again gives the moment

$$M_y = 0.003704x^3 - 0.00615x^2$$
$$- 9.631x + 194.5 \ \text{in-lb} \tag{19}$$

In the case of the finite-element model, the lift is applied as concentrated forces. The forces are applied vertically at the spanwise row of grid points along the upper surface and at the quarter-chord.

Torsional Load Case

The torsional load (torque) is applied at the tip of the spar. The torque is constant with respect to length and is selected to be

$$M_x = 50.0 \ \text{in-lb} \tag{20}$$

For the finite-element model, the torque is divided equally among the nodes at the tip and is applied as concentrated moments. An end rib composed of shear elements is used in this load case to prevent excessive distortion of the cross section. These elements provide no resistance to warping in the axial direction.

Calculation of Deflections for Coupled-Beam Analysis

The internal beam forces (centrifugal forces, shears, and moments) are calculated for the spanwise stations by means of equations (16) to (20) and averaged over the segment length. The forces are then multiplied by the beam compliance matrix to yield beam deformation derivatives. These derivatives are integrated along the span to produce deflections.

Results

Centrifugal Load Case

In the centrifugal load case, the coupled-beam-element analysis and the finite-element model agree (fig. 3). The coupled-beam analysis predicts $-15.29°$ of twist at the tip, and the finite-element model predicts $-14.13°$ at the tip. Figure 4 depicts plotter output from the finite-element analysis showing this twist.

The difference in the twist indicated by the two analyses can be attributed to several effects. The boundary effect induced by the rigid inboard end rib has a stiffening effect on the finite-element model. The rigid element does not permit any warping of the cross section out of its plane. This locally stiffens the structure in torsion. The coupled-beam-element model used in this case assumes free warping at the root. Additionally, the rigid element does not permit Poisson contraction at the root. This has a local stiffening effect in extension, and thus reduces the twist associated with extension. The coupled-beam analysis assumes free Poisson contraction. These local root stiffening effects are apparent in figure 5. The effects begin to die out at approximately radial station 10 in.

The coupled response of the spar, outboard of radial station 10 in., shows good agreement between the two analyses. (See fig. 5.) The constant offset between the two curves can most likely be attributed to wall thickness considerations. The coupled-beam analysis is a thin-wall analysis that does not include the composite-plate torsional stiffness. The finite-element model includes this stiffness.

Lifting Load Case

The two analyses also agree well on vertical deflections due to combined lift and blade weight. The coupled-beam analysis predicts 6.70 in. of deflection at the spar tip. The finite-element analysis predicts 6.48 in. of deflection at the tip. (See fig. 6.) The deflection predicted by the coupled-beam analysis is greater than that predicted by the finite-element analysis.

The coupled-beam analysis indicates that spar twist is uncoupled from both shear and bending (fig. 7). The finite-element analysis indicates a small coupling that can be considered as insignificant for design purposes (fig. 7).

Torsional Load Case

In the applied-torque case agreement is also good. Through use of equations (13) and (20), twist ϕ at the spar tip can easily be expressed for $N_x = 0$ as follows:

$$\begin{aligned} \phi &= S_{44} M_x L (180/\pi) \\ &= (0.2003 \times 10^{-3}) \ (50.0) \ (30.0) \ (180/\pi) \\ &= 17.2° \end{aligned}$$

The twist predicted by the finite-element model is distorted at the tip because of the concentrated moments at the end nodes. (See fig. 8.) The apparent excellent agreement of the two analyses at the tip is due to this distortion. The true agreement between the methods is better shown in the twist rate curve. (See fig. 9.) Again, the constant offset between the two curves in figure 9 can most likely be attributed to wall thickness considerations.

Comparison to Engineering Beam Theory

Bernoulli beam theory gives us the uncoupled relationship between beam curvature $B_{,x}$, bending moment M, and bending stiffness EI as

$$B_{,x} = M/EI$$

A similar statement can be made for the composite beam if coupling effects are ignored. If the beam chordwise shear strain is assumed to be zero, equation (6) becomes

$$B_{y,x} = \frac{M_y}{C_{55}}$$

Then C_{55} corresponds to the beam uncoupled flapwise bending stiffness EI_f. Alternately, if the chordwise shear force is taken to be zero, equation (14) becomes

$$B_{y,x} = S_{55} M_y$$

In this instance, the inverse of S_{55} corresponds to EI_f. In the case of the cantilever beam, beam strains are not constrained and bending deflections due to applied beam loads are sought. For this case it is correct to take the beam stiffness from the compliance term (S_{55}) rather than from the stiffness matrix term (C_{55}). The significance of selecting the correct term is illustrated by the particular case.

For a uniform beam with a triangular load, the deflection at the tip (ref. 5) is given as

$$z_{\text{tip}} = 11 \ w_{\text{tip}} L^4 / 120 EI_f \ \text{in.}$$

where w_{tip} is the maximum height of the triangular lift distribution. For the beam weight alone, the tip deflection is (ref. 5)

$$z_{\text{tip}} = -w L^4 / 8 EI_f \ \text{in.}$$

Superimposing the two cases and considering the 10-lb triangular lift load and given blade weight of 0.0123 lb/in. results in

$$z_{\text{tip}} = 48 \ 254.6 / EI_f \ \text{in.} \qquad (21)$$

In our particular case, C_{55} is almost twice as large as S_{55}^{-1}. Since it is not a realistic constraint to force the chordwise shear strain to zero, the beam stiffness should not be taken to be C_{55}. For our case the chordwise shear force is zero, so EI_f is taken to be S_{55}^{-1}. Substituting this value into equation (21) yields

$$z_{\text{tip}} = 6.544 \ \text{in.}$$

This value agrees well with the deflection predicted by Bernoulli beam theory and by finite-element analysis. The difference is primarily due to rounding off of the constant in the tabulated solution of reference 5. Taking the flapwise bending stiffness to be C_{55} would incorrectly indicate that the beam is twice as stiff. Similar reasoning shows that since the flapwise shear strain is not constrained, the beam

chordwise bending stiffness EI_c is taken from the compliance relationship as S_{66}^{-1}.

Since beam extension is not constrained, the torsional stiffness GK is taken from the compliance relationship as S_{44}^{-1}. Similarly, since beam twist is not constrained, the extensional stiffness EA is S_{11}^{-1}.

The engineering stiffness constants are summarized in table IV. It should be emphasized that these stiffnesses are, in general, dependent on boundary conditions and are therefore not simply cross-section properties.

Conclusions

Results from the coupled-beam theory agree well with the finite-element analysis predictions. At design rotor speed the finite-element analysis and the coupled-beam analysis indicate, respectively, 14° and 15° of twist at the spar tip. The finite-element model indicates less twist due to rigid boundary conditions and wall thickness considerations. A similar trend is indicated by the applied-torque load case. In the applied-lift load case, vertical deflections and twist indicated by both analysis methods are essentially the same. Results indicate the coupled-beam analysis is well within engineering accuracy.

The results presented demonstrate that moderate variations in spar twist can be achieved by varying the rotor rotational speed. The analysis also provides a new and convenient approach for obtaining the extensional, torsional, and bending engineering stiffnesses.

NASA Langley Research Center
Hampton, Virginia 23665-5225
December 12, 1986

References

1. Rehfield, Lawrence W.: Design Analysis Methodology for Composite Rotor Blades. *Proceedings of the Seventh Conference on Fibrous Composites in Structural Design*, AFWAL-TR-85-3094, U.S. Air Force, June 1985, pp. V(a)-1–V(a)-144. (Available from DTIC as AD B097 989L.)

2. Gockel, M. A., ed.: *MSC/NASTRAN Handbook for Dynamic Analysis—MSC/NASTRAN Version 63.* MSR-64, MacNeal-Schwendler Corp., June 1983.

3. Joseph, Jerrard A., ed.: *MSC/NASTRAN Application Manual—CDC Edition.* MSR-35(CDC), MacNeal-Schwendler Corp., Feb./Mar. 1984.

4. *MSC/NASTRAN User's Manual—MSC/NASTRAN Version 64.* MSR-39, MacNeal-Schwendler Corp., July 1984.

5. Roark, Raymond J.; and Young, Warren C.: *Formulas for Stress and Strain, Fifth ed.* McGraw-Hill, Inc., c.1975.

Table I. Orthotropic Material Properties

E_{11}, psi . . . . 23.1×10^6

E_{22}, psi . . . . 1.4×10^6

ν_{12} 0.338

G_{12}, psi . . . . 0.73×10^6

Table II. Nonzero Beam Stiffness Terms

C_{11}, lb . . . . 0.8332×10^6

C_{22}, lb . . . . 0.1651×10^6

C_{33}, lb . . . . 0.3071×10^5

$C_{44}, \text{lb-in}^2$ . . . . 0.9747×10^4

$C_{55}, \text{lb-in}^2$ . . . . 0.1337×10^5

$C_{66}, \text{lb-in}^2$ . . . . 0.1128×10^6

$C_{14}, \text{lb-in.}$ . . . . -0.6294×10^5

$C_{25}, \text{lb-in.}$ . . . . 0.3147×10^5

$C_{36}, \text{lb-in.}$ . . . . -0.3147×10^5

Table III. Nonzero Beam Compliance Terms

S_{11}, lb^{-1} . . . . 0.2345×10^{-5}

S_{22}, lb^{-1} . . . . 0.1099×10^{-4}

S_{33}, lb^{-1} . . . . 0.4561×10^{-4}

$S_{44}, \left(\text{lb-in}^2\right)^{-1}$ . . . . 0.2003×10^{-3}

$S_{55}, \left(\text{lb-in}^2\right)^{-1}$ . . . . 0.1356×10^{-3}

$S_{66}, \left(\text{lb-in}^2\right)^{-1}$ . . . . 0.1242×10^{-4}

$S_{14}, (\text{lb-in.})^{-1}$ . . . . 0.1513×10^{-4}

$S_{25}, (\text{lb-in.})^{-1}$ . . . . -0.2585×10^{-4}

$S_{36}, (\text{lb-in.})^{-1}$ . . . . 0.1273×10^{-4}

Table IV. Summary of Beam Uncoupled Engineering Stiffness Constants

Engineering stiffness constant	Compliance term	Stiffness term
Extensional, EA	S_{11}^{-1}	$\left(C_{11} - \dfrac{C_{14}^2}{C_{44}}\right)$
Torsional, GK	S_{44}^{-1}	$\left(C_{44} - \dfrac{C_{14}^2}{C_{11}}\right)$
Flapwise bending, EI_f	S_{55}^{-1}	$\left(C_{55} - \dfrac{C_{25}^2}{C_{22}}\right)$
Chordwise bending, EI_c	S_{66}^{-1}	$\left(C_{66} - \dfrac{C_{36}^2}{C_{33}}\right)$
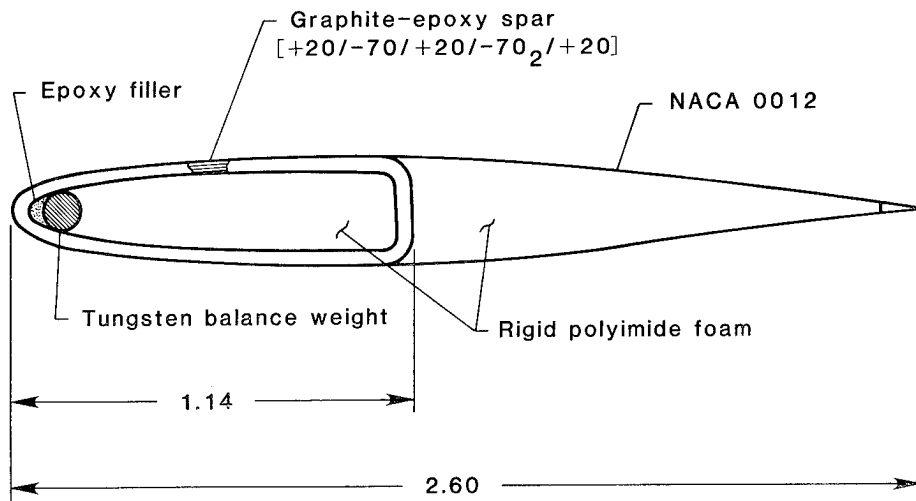
Figure 1. Model rotor cross section. Dimensions are in inches.
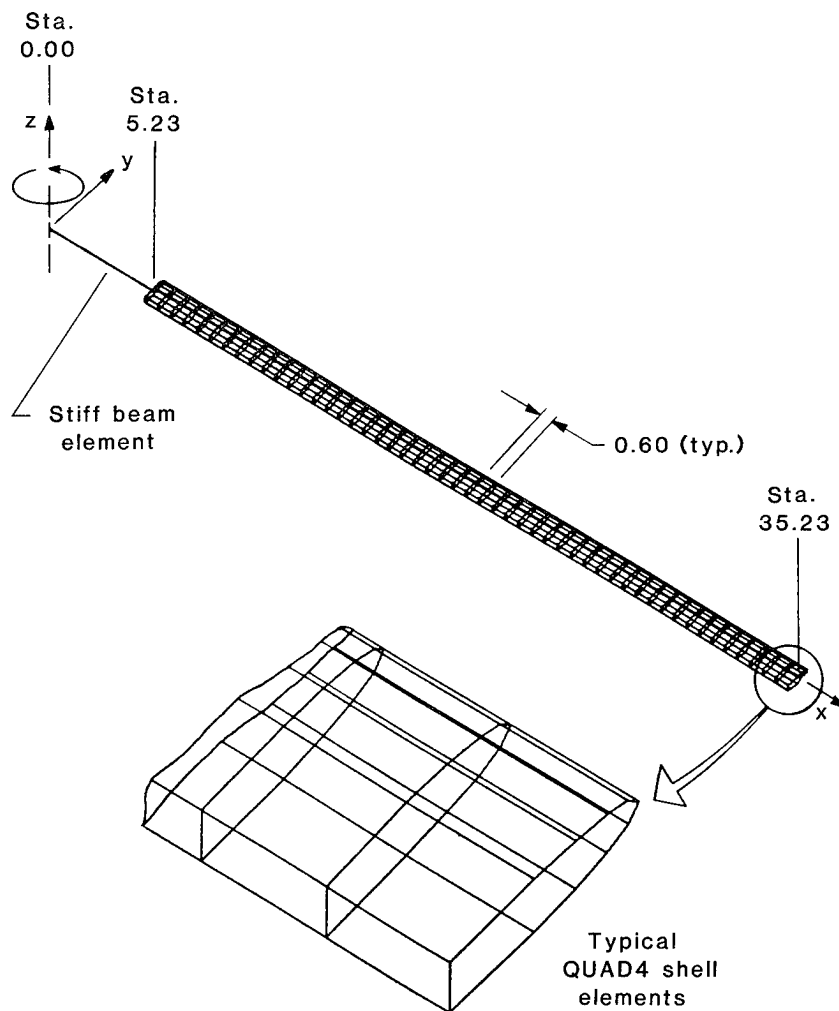
Figure 2. Model rotor spar design. Dimensions are in inches.

8
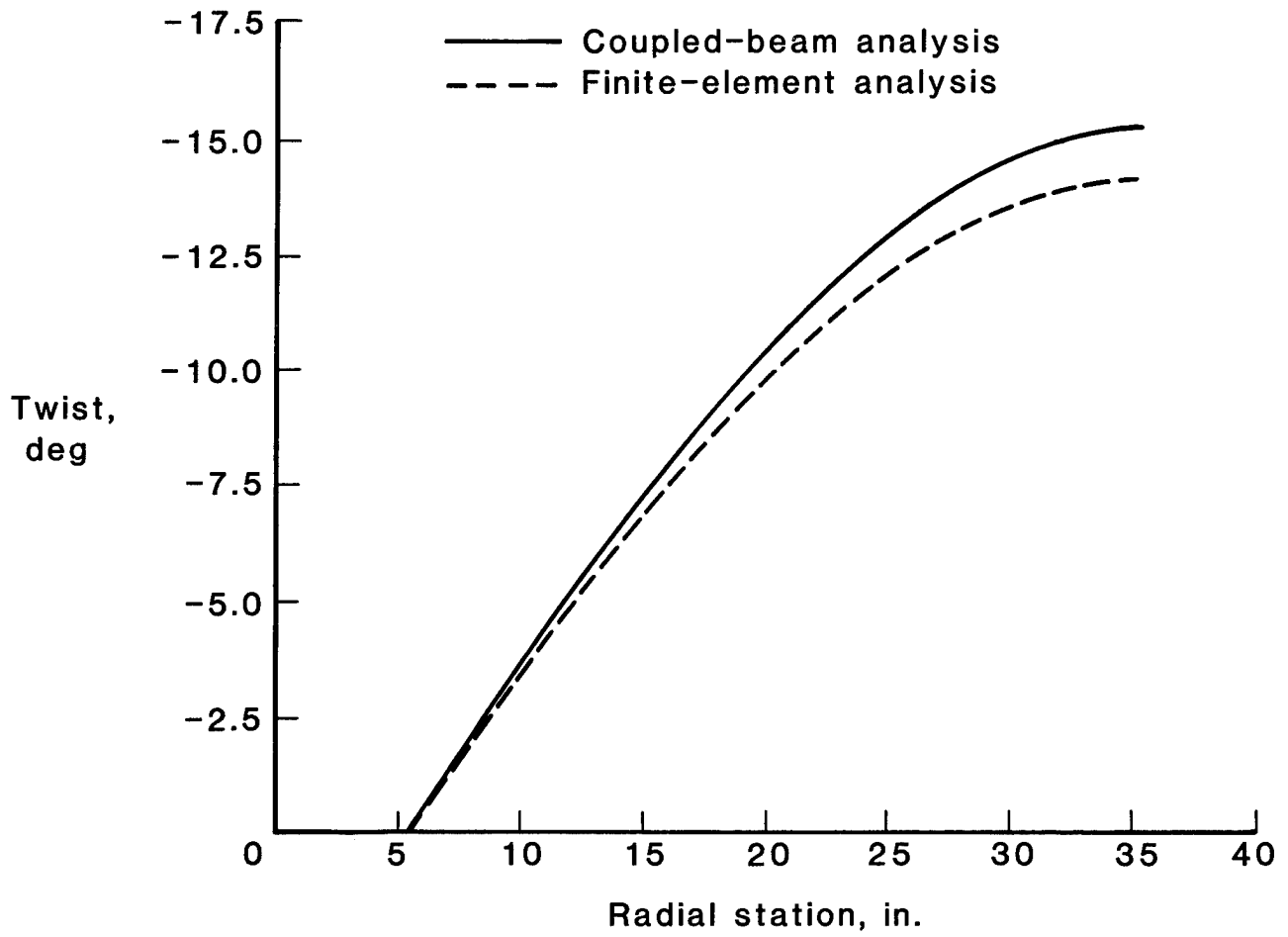
Figure 3. Twist due to centrifugal force.
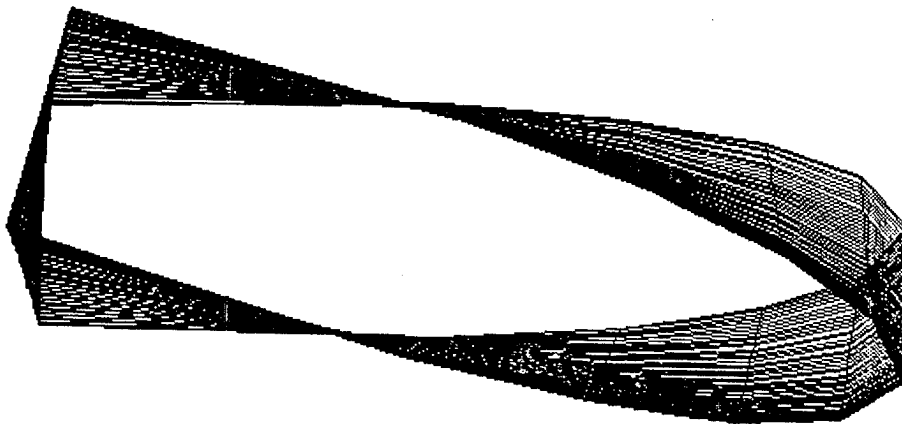
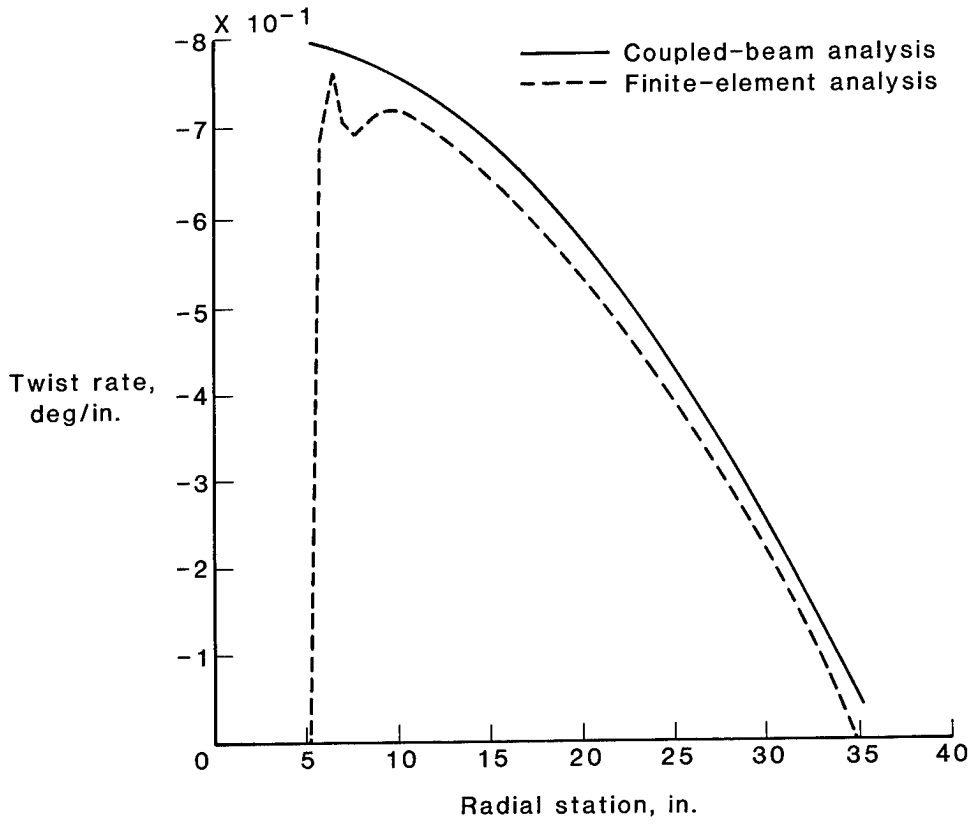Figure 4. Finite-element model twist due to centrifugal force.

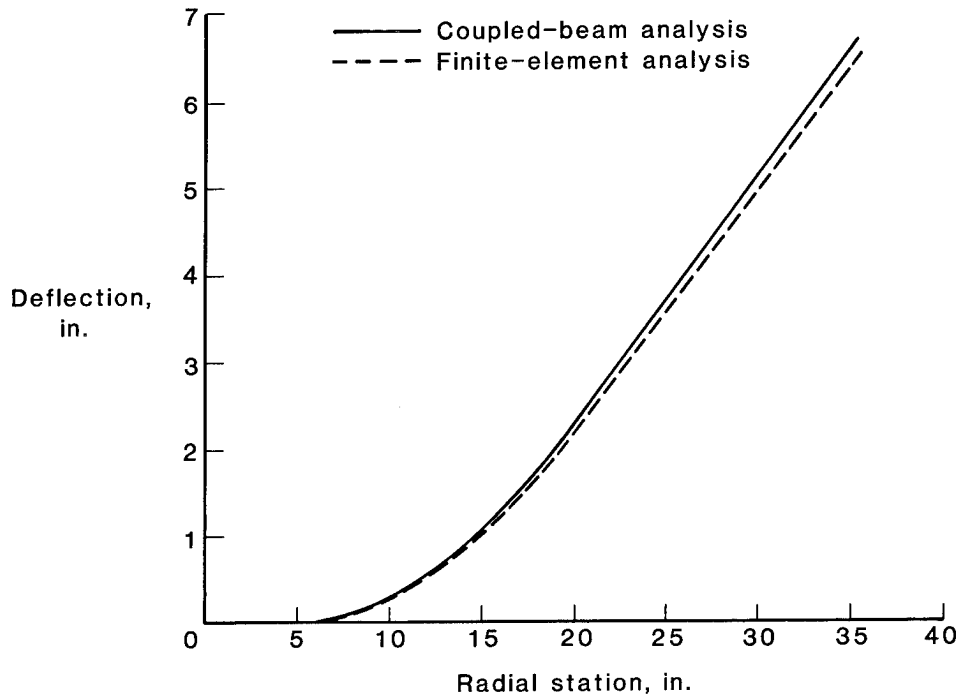Figure 5. Twist rate due to centrifugal force.

Figure 6. Beam deflection due to lift and blade weight.
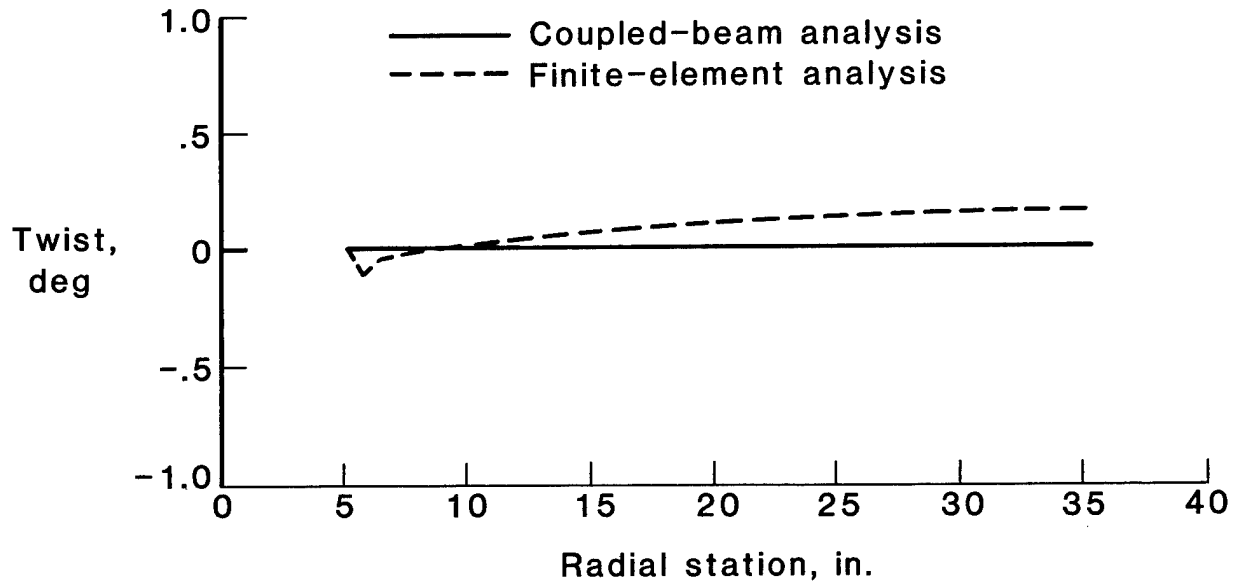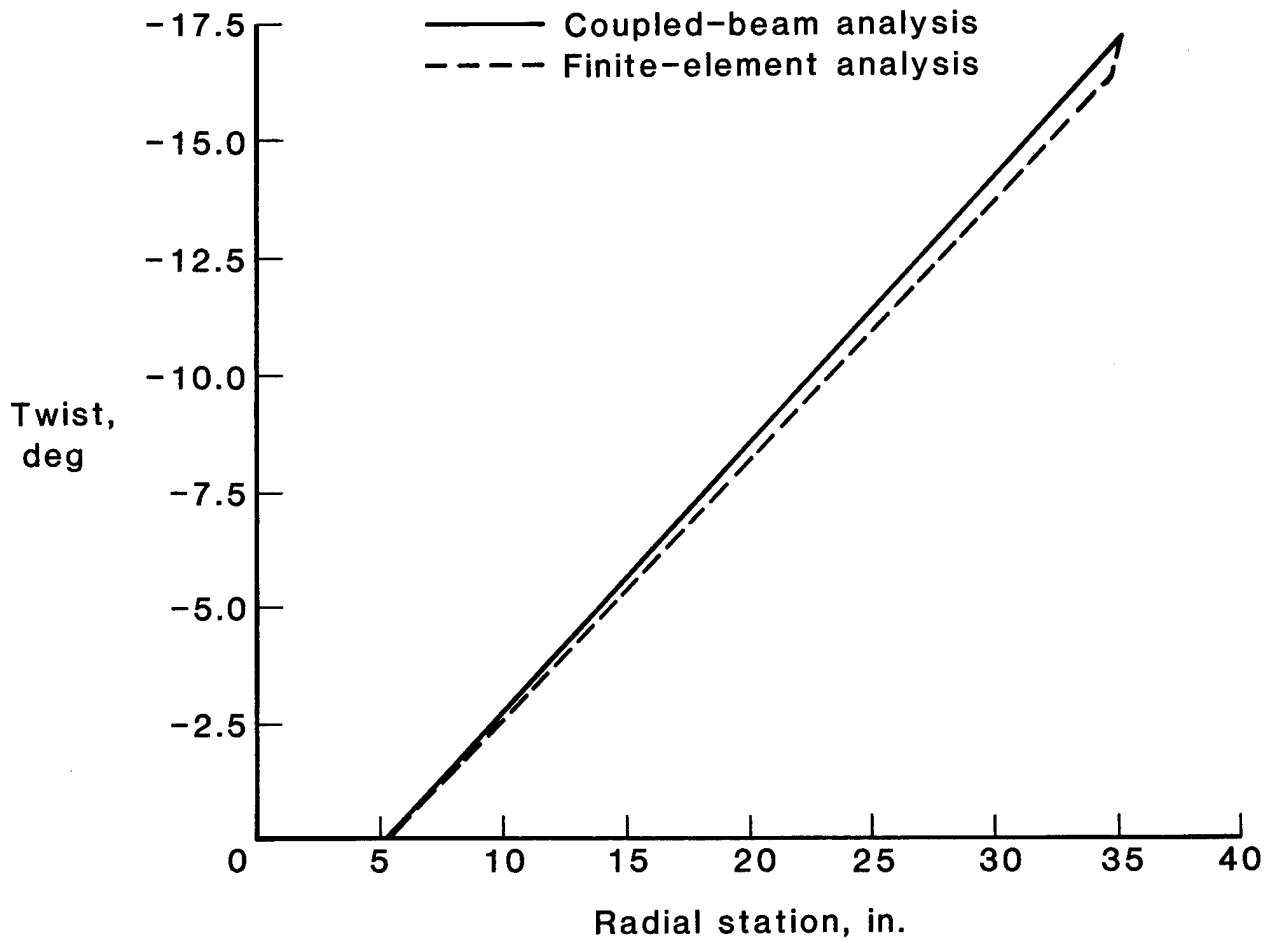
Figure 7. Twist due to lift and blade weight.
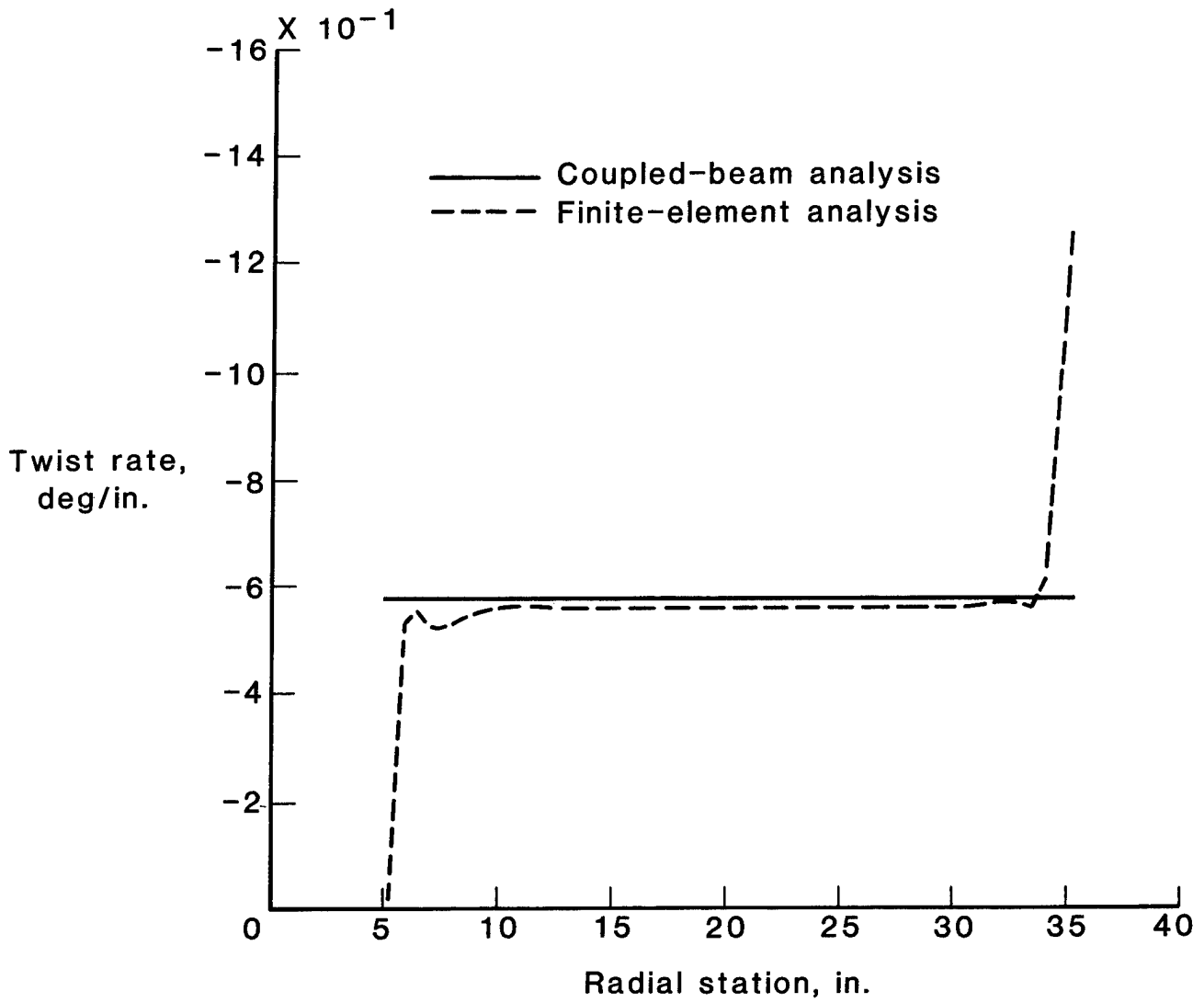

Figure 8. Twist due to applied torque.

Figure 9. Twist rate due to applied torque.

Standard Bibliographic Page

1. Report No. NASA TM-89024 AVSCOM TM-87-B-2	2. Government Accession No.	3. Recipient's Catalog No.
4. Title and Subtitle Comparison of Composite Rotor Blade Models: A Coupled-Beam Analysis and an MSC/NASTRAN Finite-Element Model		5. Report Date March 1987
		6. Performing Organization Code 505-61-59-03
7. Author(s) Robert V. Hodges, Mark W. Nixon, and Lawrence W. Rehfield		8. Performing Organization Report No. L-16207
9. Performing Organization Name and Address Aerostructures Directorate USAARTA-AVSCOM NASA Langley Research Center Hampton, VA 23665-5225		10. Work Unit No.
		11. Contract or Grant No.
12. Sponsoring Agency Name and Address National Aeronautics and Space Administration Washington, DC 20546-0001 and U.S. Army Aviation Systems Command St. Louis, MO 63120-1798		13. Type of Report and Period Covered Technical Memorandum
		14. Army Project No. 1L161102AH45

15. Supplementary Notes

Robert V. Hodges and Mark W. Nixon: Aerostructures Directorate, USAARTA-AVSCOM.
Lawrence W. Rehfield: Georgia Institute of Technology, Atlanta, Georgia.

16. Abstract

A methodology was developed for the structural analysis of composite rotor blades. This coupled-beam analysis is relatively simple to use compared with alternative analysis techniques. The beam analysis was developed for thin-wall single-cell rotor structures and includes the effects of elastic coupling. This paper demonstrates the effectiveness of the new composite-beam analysis method through comparison of results of the coupled-beam analysis with those of an established baseline analysis technique. The baseline analysis is an MSC/NASTRAN finite-element model built up from anisotropic shell elements. Deformations are compared for three linear static load cases of centrifugal force at design rotor speed, applied torque, and lift for an ideal rotor in hover. A D-spar designed to twist under axial loading is the subject of the analysis. Results indicate the coupled-beam analysis is well within engineering accuracy.

17. Key Words (Suggested by Authors(s)) Composite structure Elastic tailoring Extension-twist coupling Finite-element analysis Structural coupling analysis	18. Distribution Statement Unclassified—Unlimited Subject Category 24		
19. Security Classif.(of this report) Unclassified	20. Security Classif.(of this page) Unclassified	21. No. of Pages 14	22. Price A02